Acta Geophysica (2024) 72:273–286
https://doi.org/10.1007/s11600-023-01110-8

RESEARCH ARTICLE - APPLIED GEOPHYSICS

Pore structure characterization and deliverability prediction of fractured tight glutenite reservoir based on geophysical well logging

Tingting Hu[1] · Tuo Pan[1] · Liang Chen[1] · Jing Li[1] · Yu Liu[1]

Received: 21 February 2023 / Accepted: 3 May 2023 / Published online: 22 May 2023
© The Author(s) under exclusive licence to Institute of Geophysics, Polish Academy of Sciences & Polish Academy of Sciences 2023

Abstract
Tight glutenite reservoirs characterization and effective hydrocarbon-bearing formation identification faced great challenge due to ultra-low porosity, ultra-low permeability and complicated pore structure. Fracturing fracture-building technique always needed to obtain deliverability because of poor natural productive capacity. Pore structure characterization and friability prediction were essential in improving such type of reservoir evaluation. In this study, fractured tight glutenite reservoirs in Permian Jiamuhe Formation that located in northwest margin of Junggar Basin, northwest China, were chosen as an example, and 25 typical core samples were drilled and simultaneously applied for mercury injection capillary pressure (MICP), nuclear magnetic resonance (NMR) and whole-rock mineral X-ray diffraction experiments. A novel method of synthetizing pseudo-pore-throat radius (R_c) distribution from porosity frequency spectra was established to characterize fractured formation pore structure. Quartz and calcite were considered as the fragile mineral, and rock mineral component ratio method was used to predict brittleness index. Meanwhile, the statistical model raised by Jin et al. (SPE J 20:518–526, 2015) was used to predict two types of fracture toughness. And then, brittleness index and fracture toughness were combined to characterize tight glutenite reservoirs friability. Combining with maximal pore-throat radius (R_{max}, reflected rock pore structure) and friability, our target formations were classified into four clusters. In addition, relationships among pore structure, friability and daily hydrocarbon production per meter (DI) were analyzed, and a model to predict DI from well-logging data was established. Comparison of predicted DI with the extracted results from drill stem test (DST) data illustrated the reliability of our raised models. This would be valuable in determining optimal hydrocarbon production intervals and formulating reasonable developed plans.

Keywords Tight glutenite reservoirs · Friability · Pore structure characterization · Deliverability prediction

Introduction

Permian Jiamuhe Formation in northwest margin of Junggar Basin, China, developed a large set of tight glutenite, and the thickness ranged from 108.0 to 154.0 m (Liang et al. 2021). Compared with conventional formations, our target glutenite reservoirs contained such characteristics of ultra-low porosity, ultra-low permeability, complicated pore structure and strong heterogeneity. Core-derived porosity ranged from 5.0 to 17.0%, and the average porosity was 9.64% (Fig. 1a), permeability distributed from 0.03 to 5.01 mD, and the average permeability was only 0.15 mD (Fig. 1b), the relationship between them was poor (Fig. 1c). In addition, fractures were well developed, and this improved the seepage capability. All these made the difficulty of identifying effective reservoirs, determining "sweet spot" area and predicting hydrocarbon deliverability based on common method (Jiang et al. 2022a, b). Generally, characterizing pore structure was an effective method in improving tight reservoirs evaluation and predicting permeability (Coates et al. 2000; Dunn et al. 2002; Li et al. 2021; Gui et al. 2022; Jiang et al. 2018, 2022a, b). Many methods had been raised to characterize formation pore structure, and nuclear magnetic resonance

Edited by Dr. Liang Xiao (ASSOCIATE EDITOR) / Prof. Gabriela Fernández Viejo (CO-EDITOR-IN-CHIEF).

✉ Tingting Hu
Hutingting79@126.com

[1] Research Institute of Geophysical, Research Institute of Exploration and Development, PetroChina Xingjiang Oilfield Company, Urumchi 830013, China

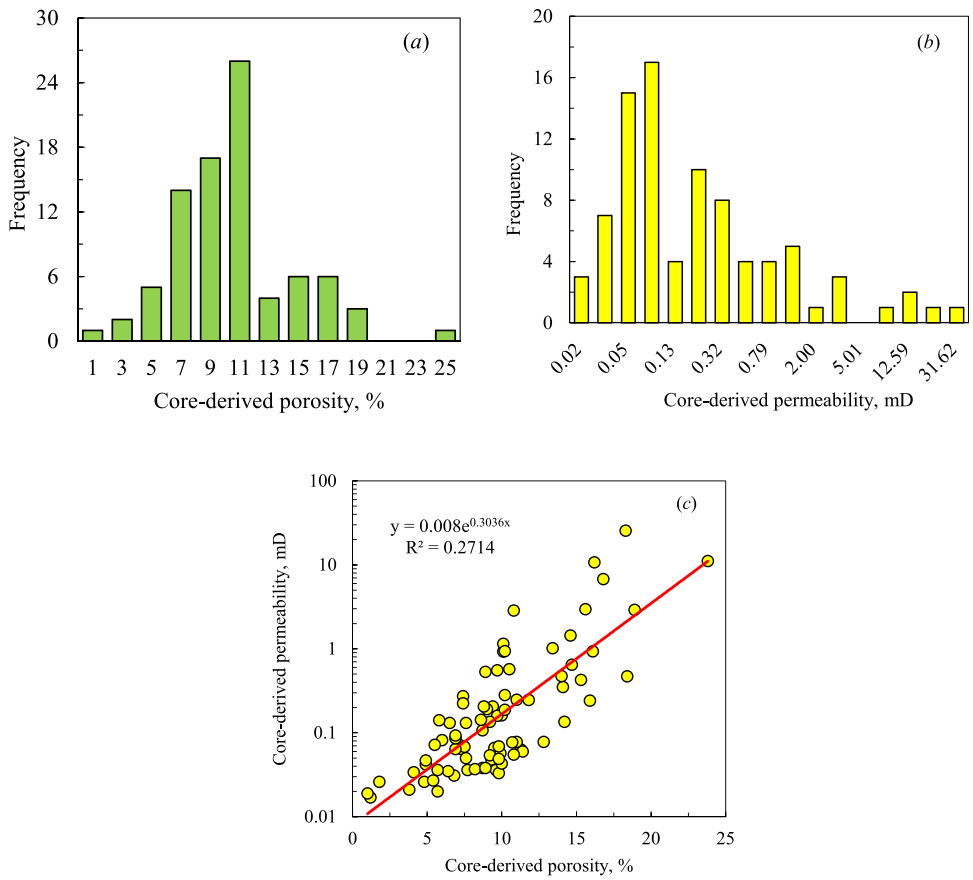

Fig. 1 Statistical histograms of core-derived porosity (**a**), permeability (**b**) and relationship between these two parameters (**c**). These figures illustrated that our target glutenite reservoirs were tight, contained complicated pore structure and strong heterogeneity

(NMR) logging was considered unique (Looyestijn, 2001; Volokitin and Looyestijn 2001; Green et al. 2008; Shao et al. 2009; Olubunmi and Chike 2011; Xiao et al. 2016; Gao et al. 2023). Looyestijn (2001) and Volokitin and Looyestijn (2001) raised a linear calibration method to construct pseudo-capillary pressure (P_c) curve from NMR logging. Afterward, the constructed pseudo-P_c was used to displace experimental mercury injection capillary pressure (MICP) curve to characterize formation pore structure. This method had been widely used in the last 20 years and was verified to be valuable in conventional clastic formation with relative high porosity and permeability. However, in low permeability sandstones, pore structure should be overestimated (Xiao et al. 2016). Although Looyestijn (2001) analyzed the reason and proposed a modified model to characterize low permeability to tight sandstone reservoirs pore structure, the theoretical basis was lacked, and the results were not obviously improved. Kuang et al. (2010) and Xiao et al. (2016) raised a model to enhance formation pore structure characterization based on piecewise power function, and the predicted results were valuable in water saturated layers. However, in hydrocarbon-bearing formations, NMR T_2 spectra were always affected by saturated hydrocarbon, and these made NMR data lose its advantage (Mao et al. 2007; Xiao et al. 2018). If we recklessly used NMR logging to characterize formation pore structure, the validity would be overestimated. In addition, fracture was developed in our target glutenite, NMR logging cannot be used in such type of formation due to slight responses of fracture to T_2 spectrum (Xiao et al., 2011). To effectively characterize fractured formation pore structure, Dong et al. (2019) and Xiao et al. (2020) proposed that electrical image logging can be used to replace NMR logging to synthesize pseudo-P_c curve, and estimate pore structure parameters. Although these methods had been verified to be effective in predicting fractured formation permeability, plenty of intermediate process of calculation made the accuracy much decrease. Meanwhile, pore structure was only characterized to predict permeability and classify formation, and relationship between pore structure and hydrocarbon deliverability was not deeply researched.

Generally, tight reservoirs did not contain natural hydrocarbon production capability, fracturing fracture-building technique was indispensable, and friability was essential (Razaz et al. 2020). Geophysical well-logging data were valuable (Kim et al. 2019). Two aspects needed to be considered in evaluating formation friability: brittleness index (BI) and fracture toughness. Brittleness index reflected the ability of cracks to crack, and crack propagation after rock was subjected to pressure. Generally, easily fractured formations tended to have a high BI, and vice versa. On the

contrary, fracture toughness reflected the ability of rocks to block hydraulic fracturing and avoid creating new and continuously expanding cracks. These two parameters were inversely proportional. Investigation that focused on BI prediction was deeply, and it was commonly used to characterize friability and reservoir quality (Jarvie et al. 2007; Rickman et al. 2008; Hucka and Das 1974; Altindag 2003; Dubey et al. 2019; Wood 2022; Ye et al. 2022). Generally, BI was associated with lithology and rock mechanics. Plenty of methods have been raised to predict BI from well-logging data, as listed in Table 1.

Here, V_{qa}, V_{ca}, V_{do} and V_{cl} are the constituent content of quartz, calcite, dolomite and clay, and separately, the unit of them is %. ΔE is the normalized Young's modulus, and Δv is the normalized Poisson's ratio, and they were all dimensionless. ε_{rs}, ε_t, ε_{irs}, ε_p and ε_r are the recoverable strain, total strain, non-recoverable strain and residual strain with dimensionless. σ_c and σ_t are the uniaxial compression and uniaxial tensile strength in MPa; λ and μ are the Ramey coefficient and shear modulus.

In the model raised by Rickman et al. (2008), ΔE and Δv were calculated from rock mechanics parameters:

$$\Delta E = \frac{E - E_{\min}}{E_{\max} - E_{\min}} \tag{1}$$

$$\Delta v = \frac{v_{\max} - v}{v_{\max} - v_{\min}}, \tag{2}$$

where E, $E_{\min}$ and $E_{\max}$ are the measured, minimum and maximum dynamic Young's modulus, respectively, and their unit was GPa. v, $v_{\min}$ and $v_{\max}$ are the measured, minimum and maximum dynamic Poisson's ratio, respectively.

Although Table 1 lists several methods that can be used to predict BI from well-logging data, several difficulties cannot be overcame: (1) Mineral type should be first analyzed by whole-rock mineral X-ray diffraction experiment. (2) Many special experiments, such as rock acoustic measurement and triaxial stress analysis, should be applied to acquire Young's modulus, Poisson's ratio and other parameters, and this was difficult. In our target formation, no rock acoustic and triaxial stress experimental data were acquired. (3) Many used parameters cannot be directly acquired, and complicated calculation process enlarged the systematic error.

There were three types of fracture expansion after the hydraulic method was used, which were the opening-type, staggered-type and tearing-type. In tight hydrocarbon-bearing formations, the opening-type (Mode-I) and staggered-type (Mode-II) cracks were easily produced, and they were created simultaneously, but the tearing-type crack was rare (Jin et al. 2015; Yuan et al. 2017). Hence, only fracture toughness that prevented Mode-I and Mode-II fractures was calculated (Yuan et al. 2017). There were two types of methods to calculate fracture toughness, which were Brazilian disk test method in laboratory and empirical statistical method (Jin et al. 2001, 2008; Chen et al. 2015). In the Brazilian disk test method, a disk core of thickness B and radius R was first prepared, and then, a high pressure was applied to create fissures. The length and width of Mode-I and Mode-II fissures were related to the amount and angle of pressure applied. Based on experimental data, fracture toughness of Mode-I and Mode-II can be calculated. This method was not operable, and many systemic errors were introduced. This made it cannot be widely used. Yuan (2017) raised an empirical statistical method to predict fracture toughness of Mode-I and Mode-II (defined as K_{IC} and K_{IIC}, separately). Relationships between K_{IC} and K_{IIC} with geophysical well-logging data were established, and they were used to predict K_{IC} and K_{IIC} from conventional logging data. Although this method was established in a certain formation, it had been widely used, especially in regions with no experimental data which can be acquired.

The purpose of this paper was to raise a method to directly extract R_c distribution to characterize tight fractured glutenite reservoirs pore structure, quantitatively analyze the relationship among pore structure, friability and deliverability and establish a model to predict glutenite reservoir deliverability. The R_c distribution was extracted from electrical image logging porosity frequency spectrum, and friability

Table 1 Methods of predicting BI from well-logging data

Method	Model	Reference
Mineral composition	$\mathrm{BI} = \frac{V_{qa}}{V_{qa}+V_{ca}+V_{do}+V_{cl}}$	Jarvie et al. (2007)
Rock mechanics parameters	$\mathrm{BI} = \frac{\Delta E+\Delta v}{2}$	Rickman et al. (2008)
Strain	$\mathrm{BI} = \frac{\varepsilon_{rs}}{\varepsilon_t}$, $\mathrm{BI} = \varepsilon_{irs} * 100\%$, $\mathrm{BI} = \frac{\varepsilon_p-\varepsilon_r}{\varepsilon_p}$	Hucka and Das (1974)
Strength	$\mathrm{BI} = \frac{\sigma_c}{\sigma_t}$, $\mathrm{BI} = \frac{\sigma_C-\sigma_t}{\sigma_c+\sigma_t}$	Hucka and Das (1974)
Strength	$\mathrm{BI} = \frac{\sigma_c\sigma_t}{2}$, $\mathrm{BI} = \frac{\sqrt{\sigma_c\sigma_t}}{2}$	Altindag (2003)
Ramey coefficient and shear modulus	$\mathrm{BI} = \frac{\lambda+2\mu}{\lambda}$	Dubey et al. (2019)

was directly estimated from conventional well-logging data. Field examples illustrated that pore structure and friability were two key factors in indicating formation validity, and they were valuable in predicting deliverability.

Method to characterize fractured tight glutenite reservoir pore structure

Theory of extracting pore-throat radius from electrical image logging

At present, the electrical image logging data were acquired from some special tools, such as the Schlumberger's formation microresistivity scanning image logging (FMI) tool or Halliburton's X-tended range micro imager (XRMI) tool. In our target region, electrical image logging was mainly acquired from FMI tool, we would introduce the theory of extracting pore-throat radius from electrical image logging that acquired by using FMI tool. FMI tool had 8 positioning arms that evenly distributed in a 360-degree range around the well. In every positioning arm, 24 button electrodes were arranged in two rows. Hence, there were total 192 button electrodes around the borehole. This can be approximated as dividing borehole into 192 tiny units (Fig. 2). Once these button electrodes were energized, 192 electrical conductivity curves can be acquired. For every tiny formation unit, the porous media can be considered that it was constructed only by intergranular pores. Secondary interstice, such as fracture and cave, can be ignored. Meanwhile, shallow investigation depth of FMI tool made the saturated pore fluid in flushed zone was mud filtrate. Relationship among formation resistivity, mud filtrate resistivity, water saturation and porosity in flushed zone can be written by Archie's equation (Archie 1942).

$$\varphi^m = \frac{abR_{\mathrm{mf}}}{S_{\mathrm{xo}}^n R_{\mathrm{xo}}}, \tag{3}$$

where S_{xo} is the flushed zone water saturation in v/v. R_{xo} is the flushed zone formation resistivity, and R_{mf} is the mud filtrate resistivity, and the unit of them was Ωm. a, b, m and n are the parameters that are associated with rock resistivity.

The investigation depth of FMI tool was closed to that of the microresistivity logging, and Eq. 3 established based on microresistivity logging can be directly used. After 192 electrical conductivity data were substituted into Eq. 3, a derivative equation can be acquired to calculate 192 apparent porosities around borehole.

$$\begin{aligned}\varphi_{i,\mathrm{FMI}} &= \sqrt[m]{\frac{abR_{\mathrm{mf}}}{S_{\mathrm{xo}}^n R_{\mathrm{xo}}}} = \sqrt[m]{\frac{abR_{\mathrm{mf}}}{S_{\mathrm{xo}}^n R_{\mathrm{xo}}}} * R_{\mathrm{xo}} * K * C_i \\ &= \sqrt[m]{\varphi^m * R_{\mathrm{xo}} * K * C_i} \\ &= \varphi * k' * \sqrt[m]{R_{\mathrm{xo}} * C_i},\end{aligned} \tag{4}$$

where C_{i} is the measured ith electrical conductivity, S/m. $\varphi_{\mathrm{i,FMI}}$ is the calculated ith porosity by using electrical conductivities. K is the proportionality coefficient between R_{xo} and C_{i}, and it was a constant. K' is the square root of K.

Theoretically, the calculated $\varphi_{\mathrm{i,FMI}}$ was a fixed value in homogeneous formation due to the close relationship between R_{xo} and C_{i}. However, $\varphi_{\mathrm{i,FMI}}$ was various and fluctuated around φ, because $R_{\mathrm{xo}}{*}C_{\mathrm{i}}$ was not a constant. The more heterogeneous the formation was, the more violent the porosity fluctuated. If we normalized $\varphi_{\mathrm{i,FMI}}$ from 0.0 to 100.0% and calculated the frequency of $\varphi_{\mathrm{i,FMI}}$ occurrence in each porosity unit, a porosity frequency histogram would be acquired (Fig. 3). After this technique was applied to process FMI logging, and porosity frequency histogram was smooth-filtered, the porosity frequency spectra can be consecutively obtained.

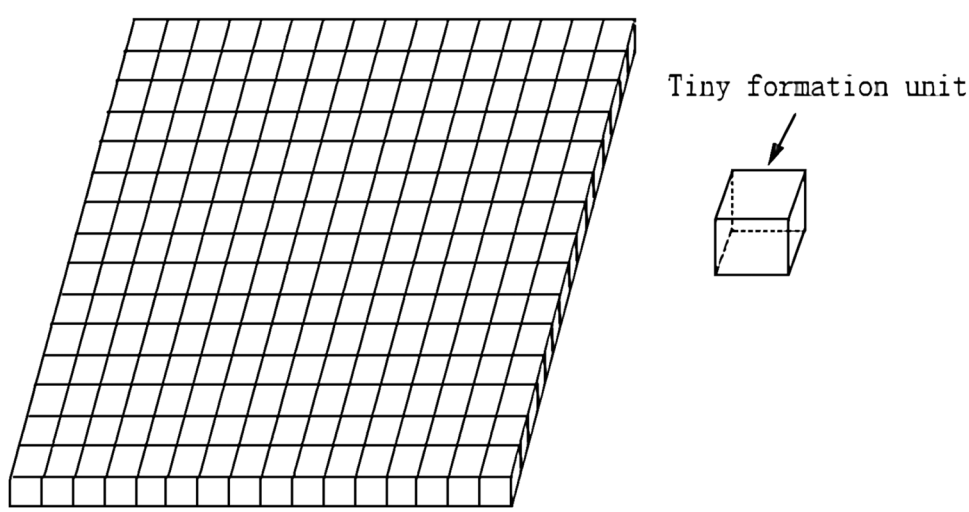

Fig. 2 Formation were divided into 192 tiny units around borehole by button electrodes

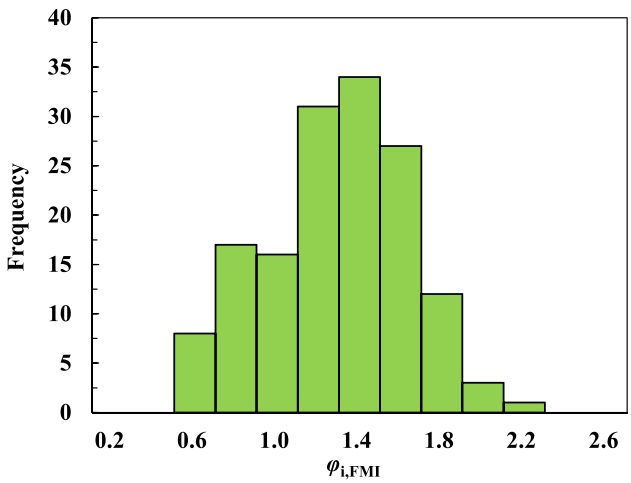

Fig. 3 The porosity frequency histogram acquired from FMI logging

Morphology comparison of porosity frequency spectrum and pore-throat radius distribution

Porosity frequency spectra can well reflect formation heterogeneity and pore structure. In strongly heterogeneous formation, e.g., carbonate or volcanic formation with secondary porosity, porosity frequency spectrum had wide bimodal distribution, and the main peak located in the right, whereas the porosity frequency spectrum would be narrow unimodal, and the main peak would locate in the left in formation with relatively simple pore structure (Fig. 4a and b). R_c distribution, which is extracted from MICP curve, directly illustrated rock pore structure. For example, R_c distribution in tight reservoirs with intergranular pores was narrow and located in the left, and once formation contained good pore structure, R_c distribution would be wide unimodal (Fig. 5a and b). However, measured NMR T_2 distributions for the same core samples did not exhibit any difference (Fig. 6a and b). This comparison verified that NMR data lost its role in tight glutenite with complicated pore structure. Although the morphology of porosity frequency spectra and R_c distributions was similar in the same type of formation, the physical significance of them, especially the *x*-axis, was absolute different. We can only qualitatively analyze pore structure from porosity frequency spectra, and if we wanted to quantitatively characterize formation pore structure, the best method was to transform porosity frequency spectrum as R_c distribution. Afterward, many parameters associated with formation quality, e.g., the average pore-throat radius (R_m), the maximal pore-throat radius (R_{max}), the threshold pressure (P_d), can also be calculated.

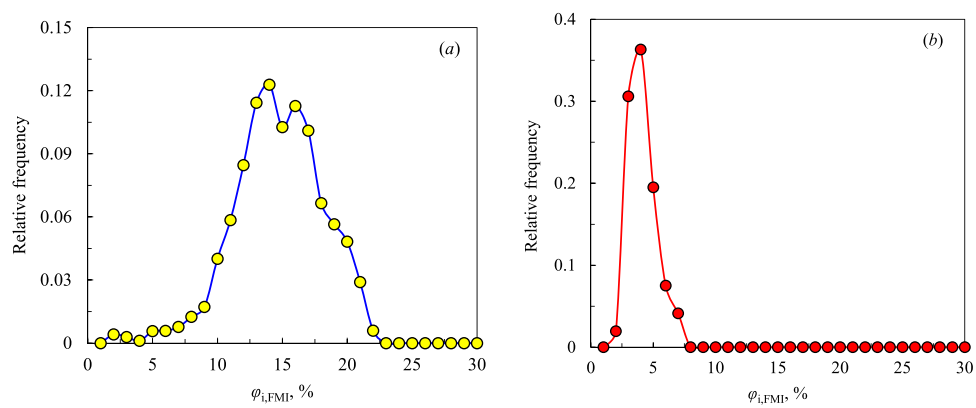

Fig. 4 Porosity frequency spectra of two types of rock in our target formation. Rock with good pore structure contained wide bimodal porosity frequency spectrum (**a**) and the porosity frequency spectrum in tight rock with poor pore structure presented as narrow unimodality (**b**)

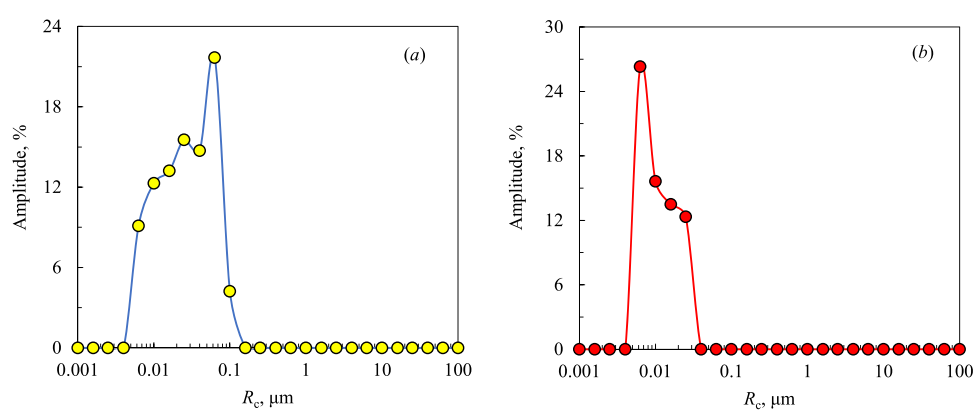

Fig. 5 R_c distributions of two types of rock in our target formation. Bimodal R_c distribution corresponded to high-quality rock (**a**). However, R_c distribution would be unimodal in tight rock (**b**)

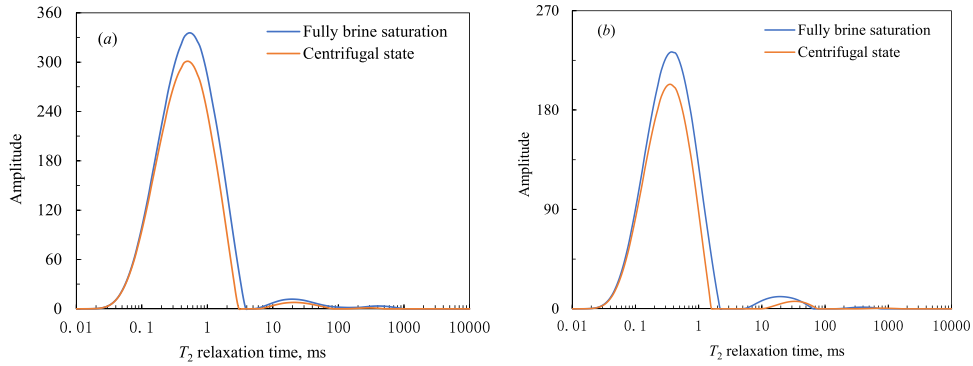

Fig. 6 NMR T_2 spectra of two types of rock in our target formation. The NMR T_2 distributions exhibited no change in different type of rocks

Method of transforming porosity frequency spectra as R_c distribution

The physical significance of y-axis in Figs. 4a and 5a was similar, it reflected the probability that porosity or pore throat appeared in a certain scope, and if we wanted to acquire R_c distribution from porosity frequency spectrum, relationship between $\varphi_{\mathrm{i,FMI}}$ and R_c should be established. In this study, a cumulative amplitude matching method was raised to extract $\varphi_{\mathrm{i,FMI}}$ under every pore-throat radius ($R_c(i)$). This method covered following procedures:

(1) Normalizing the amplitude of R_c distribution, and cumulating the normalized R_c amplitude from 0.0 to 100.0% with $R_c(i)$ increased from minimal to maximal value to get a cumulative R_c relative amplitude (Fig. 7a).
(2) Normalizing the frequency of porosity spectrum, and cumulating the normalized porosity frequency spectrum from 0.0 to 100.0% with $\varphi_{\mathrm{i,FMI}}$ increased from 0.0 to 100.0% to get a cumulative porosity spectra relative frequency (Fig. 7b).
(3) Determining R_c and $\varphi_{\mathrm{i,FMI}}$ based on the same normalized cumulative amplitude and frequency. This meant that we first determined a certain value (e.g., 20% in Fig. 7), and severally automatic searched for R_c and $\varphi_{\mathrm{i,FMI}}$ that corresponded to this value in cumulative R_c relative amplitude and cumulative porosity spectra relative frequency. Collecting R_c and $\varphi_{\mathrm{i,FMI}}$ as a data pair to analyze the relationship between them.

By using this method, we collected several data pairs of ($\varphi_{\mathrm{i,FMI}}$, R_c) from core samples and porosity frequency spectra and displayed them in a log–log coordinate. Figure 8 exhibits the relationship between these two parameters. This figure illustrated that there were good power function relations between these two parameters, and this power function exhibited as a straight line in log–log coordinate. However, the relationships were not uniform for all core samples; for different types of core sample, the relationships were divergent. Meanwhile, in different pore-throat parts (small and large pore throat), the relationships were also varied, and this variation exhibited as segmentation.

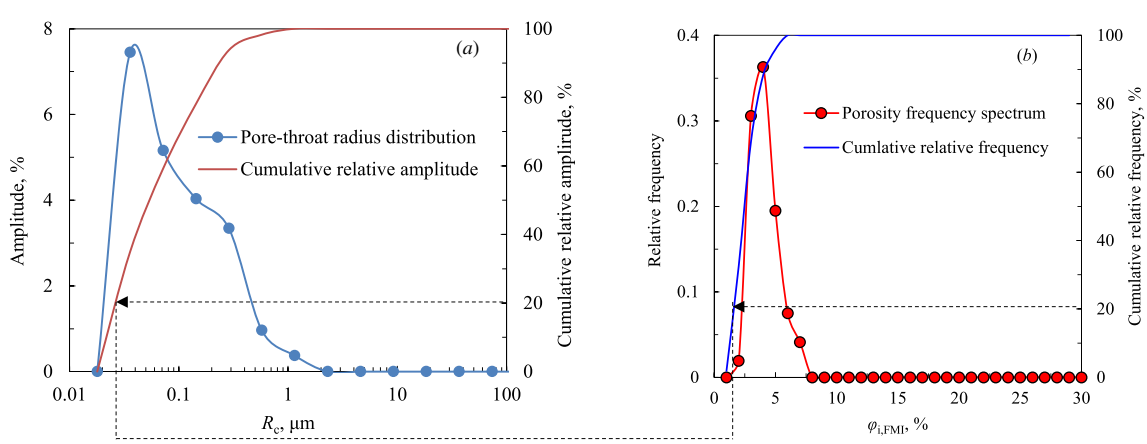

Fig. 7 Principle of determining $\varphi_{\mathrm{i,FMI}}$ that corresponded to every R_c based on cumulative amplitude matching method

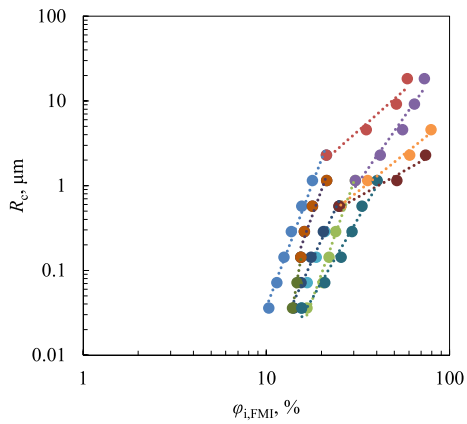

Fig. 8 Relationship between $\varphi_{i,FMI}$ and R_c for several types of core samples

Model of synthesizing R_c distribution based on formation classification

Figure 8 illustrates that power function relation existed between porosity frequency spectrum and R_c distribution for a single core sample. However, in heterogeneous formation, it was difficult to exhibit such relation by using uniform function in the whole intervals. In other words, if we only used one relation to acquire pseudo-R_c distributions from porosity frequency spectra, the pore structure characterization accuracy would deeply decrease. In this study, to extract reasonable pseudo-R_c distribution, 25 core samples were drilled from tight glutenite reservoir in Permian Jiamuhe Formation of northwest margin in Junggar Basin, northwest China, and they were simultaneously applied for mercury injection capillary pressure (MICP), NMR and whole-rock mineral X-ray diffraction experiments. R_c distributions and porosity frequency spectra were acquired. The experimental results are listed in Table 2. Based on these 25 core samples, a model of synthesizing pseudo-R_c from porosity frequency spectra based on formation classification was raised. In this model, 25 core samples were first classified into 4 clusters based on physical property difference. Second, for every type of core sample, independent power function was used to reflect the relationship between $\varphi_{i,FMI}$ and R_c. Meanwhile, in small and large pore-throat parts, two functions were, respectively, used. Third, applying the established model in field application, after formations were classified by using the same physical property criteria, consecutive pseudo-R_c distributions can be constructed in the intervals with which electrical image logging was acquired.

Model of synthesizing pseudo-R_c distributions from porosity frequency spectra based on formation classification was expressed as follows:

$$\text{Small pore-throat part: } R_c(i) = a_s * \varphi_{i,FMI}^{b_s} \quad (5)$$

$$\text{Large pore-throat part: } R_c(i) = a_l * \varphi_{i,FMI}^{b_l}, \quad (6)$$

where $R_c(i)$ is the ith pore-throat radius in μm. a_s, b_s, a_l and b_l are the involved parameters, and their values needed to be calibrated by using experimental data of core samples.

By using experimental data of 25 core samples, the involved parameters of a_s, b_s, a_l and b_l were separately calibrated for four clusters of rocks, and models of synthesizing pseudo-R_c distributions from porosity frequency spectra were established and are displayed in Fig. 9. This figure clearly indicated that good segmented power functions existed between these two parameters. Once they were extended into field application in the intervals with which porosity frequency spectra were extracted from electrical image logging, R_c distributions can be acquired to characterize tight glutenite reservoir pore structure.

Reliability verification

Models that are displayed in Fig. 9 were applied in field application to process electrical image logging, and pseudo-R_c distribution was synthetized to characterize pore structure. Further, the pore structure evaluation parameters, e.g., R_{max}, P_d, pore-throat radius corresponded to 10.0% mercury injection saturation (R10), and median pore-throat radius (R_{50}), were calculated. To verify the reliability of our raised technique, we compared the calculated pore structure parameters with core-derived results, and displayed in Fig. 10. The first three tracks of this figures displayed conventional well-logging curves, and they were used to identify effective formation, calculate porosity and identify pore fluids, separately. POR_HIST displayed in the fourth track was the porosity frequency spectra extracted from electrical image logging. RC_DIST was the synthetized pseudo-R_c distributions from porosity frequency spectra based on our raised technique and exhibited in the fifth track. RMAX, R10, PD and SWANSON displayed from the sixth to ninth tracks were the pore structure parameters calculated from pseudo-R_c distributions, separately. CRMAX, CR10, CPD and CSWANSON were the derived results from core samples. Good consistency between the calculated pore structure parameters from pseudo-R_c distributions and core-derived

Table 2 Experimental data of 25 core samples that drilled from Permian Jiamuhe Formation of northwest margin in Junggar Basin, northwest China

Core no.	Depth (m)	Mineral content (%)												
		Quartz	K-spar	Anorthose	Calcite	Dolomite	Aragonite	Siderite	Pyrite	Lomontite	Analcidite	Augite	Ankerite	Clay
1	2338.26	35.0	0.0	10.8	4.0	0.0	0.0	1.8	0.0	0.0	4.2	12.4	9.3	16.2
2	2420.27	19.8	0.0	9.1		0.0	0.0	1.4	0.0	0.0	6.2	7.1	0.0	56.4
3	2421.46	18.6	0.0	12.7	2.8	0.0	0.0	2.7	0.0	0.0	4.4	0.0	0.0	58.8
4	2424.46	12.6	0.0	18.5	5.8	0.0	0.0		0.0	0.0	1.5	14.6	11.4	35.6
5	2892.48	34.4	0.0	24.7	2.2	0.0	0.0	1.8	0.0	0.0	0.0	0.0	8.7	28.2
6	2165.25	9.1	0.0	8.6	28.3	0.0	0.0	5.4	4.7	0.0	1.0	19.2	0.0	23.7
7	2166.57	2.3	0.0	6.7	15.1	0.0	19.2	6.0	5.1	0.0	0.0	0.0	0.0	45.6
8	2167.8	12.9	0.0	5.8	15	3.2	16.6	4	2.9	0.0	0.0	0.0	0.0	39.6
9	2170.02	18.6	0.0	3.0	3.8	0.0	7.0	1.6	5.1	2.8	2.0	5.8	0.0	32.9
10	2435.31	19.0	0.0	11.6	28.3	0.0	3.8	2.4	0.0	8.5	1.7	0.0	0.0	24.7
11	2441.01	11.2	3.1	13.4	1.7	7.0	4.7	2.5	0.0	5.1	1.9	0.0	0.0	31.5
12	2455.4	20.2	3.0	20.5	16.5	0.0	3.4	2.0	0.0	7.2	0.0	0.0	0.0	16.5
13	2772.96	12.8	0.0	23.3	10.6	0.0	13.0	4.0	3.5	0.0	2.8	0.0	4.2	25.8
14	2774.8	10.7	2.2	0.0	0.0	0.0	5.9	2.2	0.0	0.0	3.5	0.0	0.0	46.8
15	2776.83	9.7	0.0	21.1	4.6	0.0	6.8	2.1	0.0	0.0	3.6	0.0	0.0	29.5
16	3405.59	2.6	0.0	19.3	2.3	21.6	0.0	0.0	0.0	0.0	0.0	0.0	19.7	34.5
17	2523.18	10.7	0.0	1.7	23.2	3.1	0.0	0.0	0.0	0.0	0.0	1.8	0.0	16.5
18	2524.1	32.7	0.0	6.7	12.0	0.0	0.0	0.0	0.0	0.0	0.0	0.0	0.0	48.6
19	2529.06	24.1	0.0	18.2	5.0	0.0	0.0	8.3	0.0	0.0	2.9	0.0	0.0	41.5
20	4002.29	26.5	4.2	44.9	11.9	0.0	0.0	0.8	0.0	5.6	0.0	0.0	0.0	6.1
21	4007.55	18.0	0.0	18.3	5.7	0.0	0.0	0.0	0.6	4.4	7.9	0.0	0.0	19.9
22	4102.07	7.0	3.7	50.4	0.9	0.0	0.0	0.4	0.6	28.3	0.0	0.0	0.0	8.7
23	4337.47	11.8	0.0	10.1	7.0	0.0	3.8	0.7	0.0	42.5	0.0	0.0	0.0	24.1
24	4843.3	1.1	0.0	21.3	0.0	26.7	0.0	2.5	0.0	0.0	3.2	0.0	0.0	45.2
25	4004.25	13.5	1.3	36.3	3.4	0.0	0.0	0.4	0.0	32.9	0.0	0.0	0.0	12.2

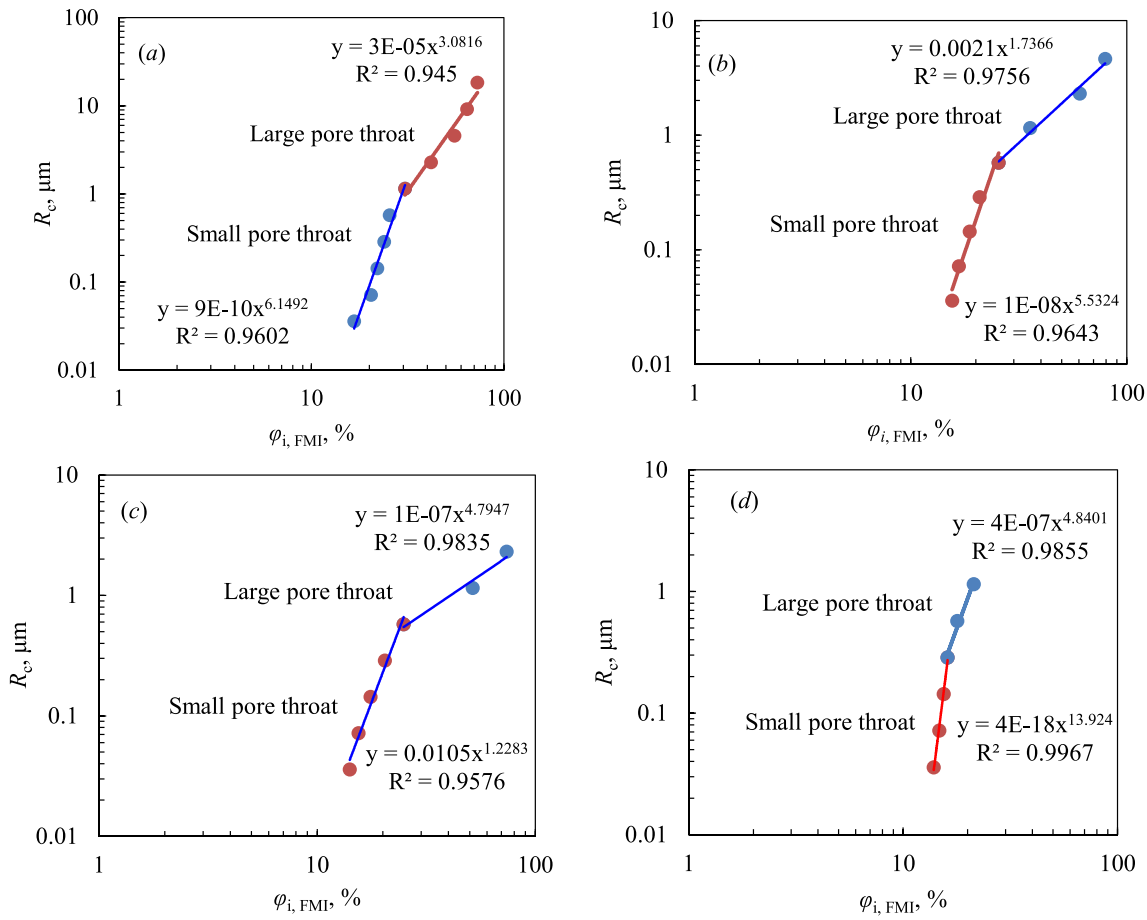

Fig. 9 Models of transforming porosity frequency spectra as R_c distribution based on formation classification method

results demonstrated the reliability of our raised technique. The synthetized pseudo-R_c distributions can be used to well characterize formation pore structure.

Estimation of tight glutenite reservoir friability

Generally, friability was affected by two aspects: positive brittleness and negative fracture toughness. Friability cannot be directly calculated, statistical methods was always used to first predict brittleness and fracture toughness from well-logging data, and then, these two parameters were combined to acquire rock friability.

Estimation of BI

Only whole-rock mineral X-ray diffraction experimental data were acquired in our target Permian Jiamuhe Formation, we would establish BI prediction model based on mineral contents in this study. Generally, quartz and carbonate were considered to be friable, and feldspar, clay and pyrite were flexible in Jiamuhe Formation (Hu 2021). Hence, a model of calculating BI based on mineral contents was established:

$$\mathrm{BI} = \frac{V_{\mathrm{qa}} + V_{\mathrm{ca}}}{V_{\mathrm{qa}} + V_{\mathrm{fd}} + V_{\mathrm{ca}} + V_{\mathrm{py}} + V_{\mathrm{cl}}}, \tag{7}$$

where BI is the brittleness index in dimensionless. V_{fd} and V_{py} are the constituent content of feldspar and pyrite, separately, and the unit of them was %.

To predict BI by using Eq. 7, V_{qa}, V_{ca}, V_{fd}, V_{py} and V_{cl} should be first acquired. In Jiamuhe Formation, based on whole-rock mineral X-ray diffraction experimental data of 25 core samples, optimization technique based on multimin module in Paradigm's Geolog software was applied, and BI was consecutively predicted from conventional well-logging data.

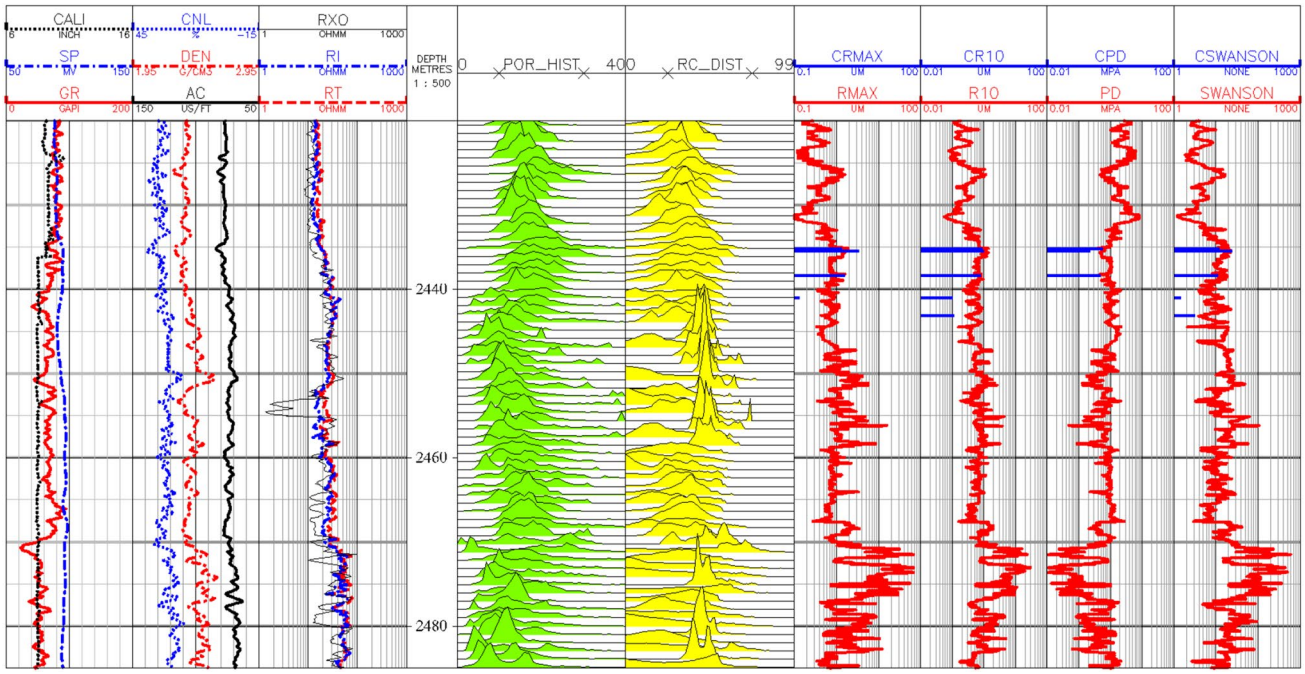

Fig. 10 Comparisons of calculated pore structure parameters from synthetized pseudo-R_c distribution with core-derived results in our target tight glutenite reservoir

Estimation of fracture toughness

In our target tight glutenite reservoirs, no core samples were used to apply for Brazilian disk experiment in laboratory, and the empirical statistical method raised by Yuan et al. (2017) was directly applied to predict fracture toughness. Models of predicting fracture toughness of Mode-I and Mode-II were expressed as follows.

$$K_{\mathrm{IC}} = 0.45 \times \rho - 0.151 \times \exp\left(V_{\mathrm{sh}}\right) + 0.201 \times \ln(AC) - 0.87 \tag{8}$$

$$K_{\mathrm{IIC}} = 2.121 \cdot \rho - 0.245 \bullet \exp\left(V_{\mathrm{sh}}\right) + 1.152 \bullet \ln(AC) - 8.378, \tag{9}$$

where K_{IC} and K_{IIC} are the fractured toughness that caused by Mode-I and Mode-II expansion of fracture. ρ is the bulk density in g/cm^3, and AC is the interval transit time in μs/m. Their values were directly acquired from conventional well-logging data. V_{sh} is the content of shaly in v/v. Its value was calculated from natural gamma ray:

$$I_{\mathrm{GR}} = \frac{\mathrm{GR} - \mathrm{GR}_{\mathrm{min}}}{\mathrm{GR}_{\mathrm{max}} - \mathrm{GR}_{\mathrm{min}}} \tag{10}$$

$$V_{\mathrm{sh}} = \frac{2^{GCUR \bullet I_{GR}} - 1}{2^{GCUR} - 1}, \tag{11}$$

where GR is the natural gamma ray in API. $\mathrm{GR}_{\mathrm{min}}$ and $\mathrm{GR}_{\mathrm{max}}$ are the minimal and maximal values of natural gamma ray in a formation in API, respectively. I_{GR} is the shale-content index. GCUR is the dimensionless Hilchie index, and its value was commonly defined as 3.7.

Friability evaluation

Based on the negative correlation between BI and fracture toughness, a parameter, named as friability, was raised. It was defined as the degree to which a rock was easily fractured. Hence, friability was positively related to BI, and negatively related to fracture toughness, and calculated as follows:

$$F_{\mathrm{rac}} = \mathrm{BI} \times \frac{1}{\alpha \times K_{\mathrm{IC}} + \beta \times K_{\mathrm{IIC}}}, \tag{12}$$

where F_{rac} is the fracability in MPa^{-1} m$^{-0.5}$. α and β are the statistical proportionality coefficient, and their values need to be calibrated and satisfied following relation: $\alpha + \beta = 1.0$. Once no calibration data were available, their values were defined as 0.5 and 0.5, separately.

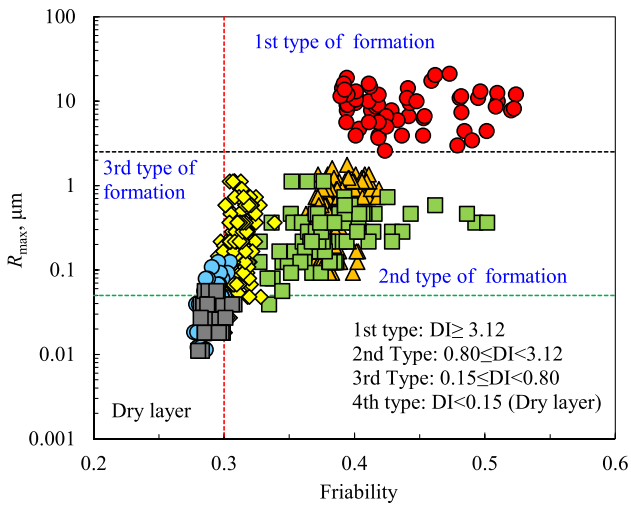

Fig. 11 Tight glutenite reservoirs validity estimation by combining with pore structure and friability

Formation validity estimation and deliverability prediction

Validity estimation

To analyze the effect of pore structure and friability to reservoir quality, 11 formations that contained drill stem test (DST) data in our target region were collected. Formation pore structure and friability were first characterized from electrical image and conventional well logging, separately. Meanwhile, daily hydrocarbon production per meter (defined as deliverability index, and expressed as DI) was used to reflect formation quality. Relationship among pore structure, friability and reservoir quality was analyzed. Finally, we found that R_{max}, F_{rac} and DI were closely related to each other. Based on DI, our target tight glutenite reservoirs were classified into four cluster (Fig. 11), and the corresponded reservoir classification criteria and DI difference are listed in Table 3. The first type of formation contained the best pore structure and highest friability and thus had the highest DI. The second type of formation had relative higher friability, but relative poorer pore structure, fracturing fracture-building technique can be used to raise hydrocarbon production. The third type of formation contained relative better pore structure but weaker friability, and stable capacity can be acquired but DI was low. Meanwhile, fracturing fracture-building technique lost its roles. The fourth type of formation was dry layer, and no liquid can be produced. Based on Fig. 11 and Table 3, the validity of our target reservoirs was evaluated, and high-quality producing pays can be well identified.

Table 3 Criteria of classifying tight glutenite reservoirs based on pore structure and friability

Reservoir type	Maximal pore-throat radius (R_{max}), μm	Friability (F_{rac})	Daily hydrocarbon production per meter (DI), m^3/(day m)	Reservoir quality
Type 1	Greater than 3.0	Greater than 0.3	Greater than 3.12	Top-quality
Type 2	0.5 ~ 3.0	Greater than 0.3	0.80 ~ 3.12	Relatively high-quality
Type 3	0.5 ~ 3.0	Lower than 0.3	0.15 ~ 0.80	Relatively low-quality
Type 4	Lower than 0.5	Lower than 0.3	Lower than 0.15	The worst

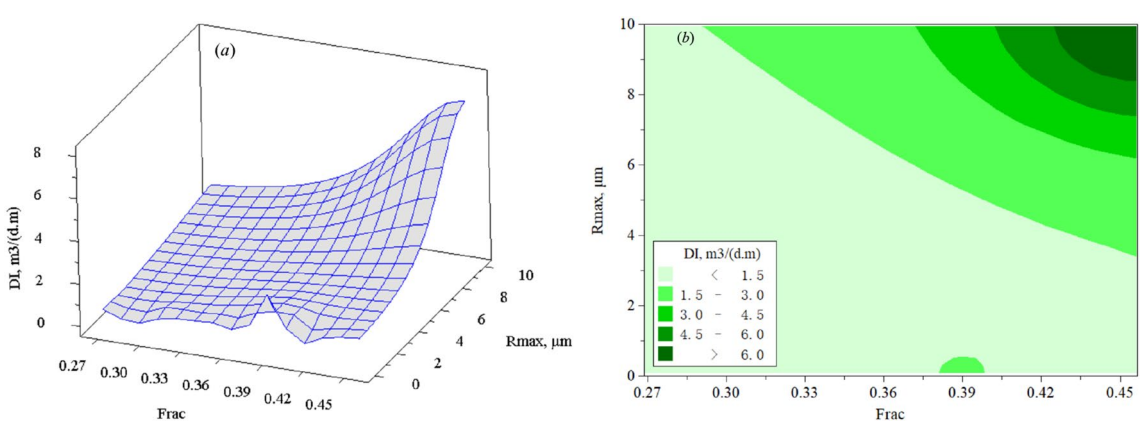

Fig. 12 3D surface graph (**a**) and contour map (**b**) of friability, maximal pore-throat radius and daily hydrocarbon production per meter of our target tight glutenite reservoir

Deliverability prediction

In formations with DST data, we used the equal area method to obtain the mean values of R_{max} and F_{rac} (defined as R_{max_m} and F_{rac_m}), and they were used to represent formation properties. Relationship among R_{max_m}, F_{rac_m} and DI was analyzed. Figure 12a and b displays this relation based on 3D surface graph and contour map, separately. It can be clearly observed that good positive correlation existed among these three parameters. With the increase of R_{max_m} and F_{rac_m}, the corresponding DI was higher. Based on this analysis, we tried to establish a model to connect these three parameters, as was expressed in Eq. 13. It should be noted that R_{max_m} was logarithmic due to large range of numerical variations. By using this model, DI can be first predicted from R_{max} and friability in the intervals with which DST data was not acquired. Once formation effective thickness was determined, hydrocarbon deliverability can be predicted. This was of great importance in exploration wells to determine the optimal production intervals and formulate the appropriate developmental plans.

$$\mathrm{DI} = 6.21 * \log_{10}^{2}\left(R_{max_m}\right) + 0.50 * \log_{10}\left(R_{max_m}\right) + 0.58 * F_{rac_m} - 1.16 \quad (13)$$

Case study

By using the established models, several wells with conventional and electrical image logging were processed in our target tight glutenite reservoirs. After pore structure was characterized by using synthetized pseudo-R_c distributions, pore structure parameters were calculated. Meanwhile, friability was also predicted from conventional well logging by using the proposed method. In addition, the daily hydrocarbon production per meter was calculated from R_{max} and F_{rac} based on Eq. 13. Figure 13 displays a field example of characterizing formation pore structure, evaluating friability and predicting formation type. The physical significance of the displayed well-logging curves in the first six tracks was the same as that displayed in Fig. 10. In the seventh track, we displayed the calculated fracture toughness of Mode-I and Mode-II, and friability curve (FRAC) was exhibited in the eighth track. In the last track, we displayed the predicted DI from R_{max} and F_{rac}. Based on R_c distribution, R_{max} and F_{rac}, it can be clearly predicted that the interval of 2156.0–2177.0 m was the highest quality in this well due to good pore structure and friability (belonged to the first type of formation in Fig. 11), and the calculated DI reached to 7.33 m^3/(day m). This prediction was verified by the DST data. In the intervals of 2138.0 ~ 2142.0 and 2164.0 ~ 2170.0 m, pure light

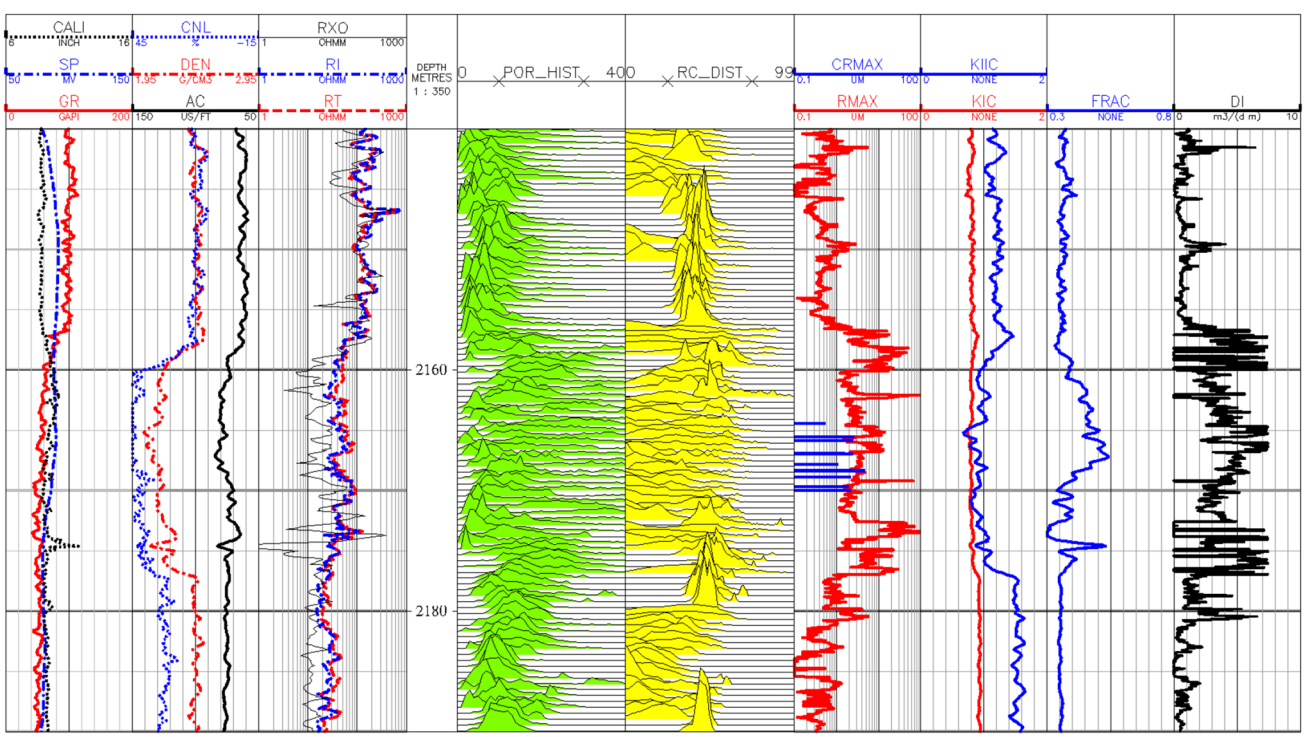

Fig. 13 A field example of characterizing formation pore structure, evaluating friability and predicting daily hydrocarbon production per meter by using our raised models

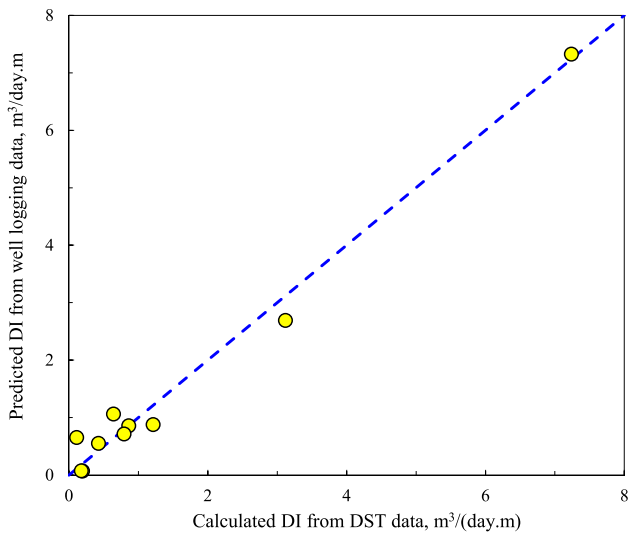

Fig. 14 Comparison of predicted DI from well-logging data based on our raised technique with the extracted results from DST data in Permian Jiamuhe Formation of northwest margin in Junggar Basin

oil was produced, and the measured DI was 7.24 m^3/(day m), and it was very closed to the predicted result.

Figure 14 compares the predicted DI from well-logging data based on our raised technique and calculated result from DSI data in 11 wells. Blue dotted line was the 45° diagonal, and it was used to reflect the deviation degree of predicted DI with that of extracted results from DST data. This figure clearly illustrated that the data points were distributed on both sides of the diagonal and meant that the predicted results were infinitely closed to the true values. This verified that our raised methods of characterizing tight glutenite reservoirs pore structure, evaluating friability and predicting DI were reliability in Permian Jiamuhe Formation. Once they were extended to formations with similar properties, DI can be well predicted, and this was of great importance in improving complicated reservoirs characterization and formulating reasonable development plans.

Conclusions

Fractured tight glutenite reservoirs pore structure characterization and friability evaluation were of great importance in improving high-quality formation identification and hydrocarbon-producing capacity prediction. The NMR logging lost its role in characterizing fractured formation pore structure, whereas the porosity frequency spectra extracted from electrical image logging were valuable.

Based on the morphological characteristics analysis of porosity frequency spectra and R_c distributions for different types of rocks, we raised a novel technique of transforming porosity frequency spectra as pseudo-R_c distributions to characterize fractured tight glutenite reservoir pore structure based on formation classification method, and the corresponding models were established. Reasonable results illustrated the reliability of our raised technique.

Brittleness index and fracture toughness were predicted from conventional well-logging data, and a parameter of friability was raised to reflect the effect of engineering scheme to formation property and deliverability.

Combining with pore structure and friability, our target tight glutenite reservoirs were classified into four clusters. Meanwhile, relationships among pore structure, friability and DI were analyzed, and a model of predicted DI from R_{max} and F_{rac} was established. Good consistency between the predicted DI and the extracted results from DST data illustrated the reliability of our raised method.

Acknowledgements This research was supported by the Major National Oil &Gas Specific Project of China (No. 2016ZX05003-005).

Author contributions TH was involved in funding acquisition, processing FMI logging and writing original draft. Tuo Pan was involved in establishing reservoir pore structure characterization method, processing 11 wells and revising draft. LC was involved in establishing techniques of predicting brittleness index, fracture toughness and evaluating rock friability. JL was involved in analyzing relationships among pore structure, friability and deliverability and estimating tight glutenite reservoirs deliverability prediction model. YL was involved in compiling computer program to automatic processing well-logging data and revising draft.

Declarations

Conflict of interest The authors declare no conflict of interest.

References

Altindag R (2003) Correlation of specific energy with rock brittleness concepts on rock cutting. J S Afr Inst Min Metall 103:163–171. https://doi.org/10.1016/S0022-3115(03)00070-9

Archie GE (1942) The electrical resistivity log as an aid in determining some reservoir characteristics. Trans AIME 146:54–62

Chen JG, Deng JG, Yuan JL, Yan W, Yu BH, Tan Q (2015) Research on the determination of type I and II of shale formation fracture toughness. Chin J Rock Mech Eng 34:1101–1105. https://doi.org/10.13722/j.cnki.jrme.2014.1187

Coates GR, Xiao LZ, Primmer MG (2000) NMR logging principles and applications. Gulf Publishing Company, Houston, pp 1–256

Dong XM, Zhang T, Yao WJ, Hu TT, Li J, Jia CM, Guan J (2019) A method to quantitatively characterize tight glutenite reservoir pore structure. In: Proceeding of SPE Reservoir Characterisation and Simulation Conference and Exhibitions. https://doi.org/10.2118/196649-MS

Dubey A, Mohamed MI, Salah M, Algarhy A (2019) Evaluation of the rock brittleness and total organic carbon of organic shale using

triple combo. In: SPWLA 60th Annual Logging Symposium. https://doi.org/10.30632/T60ALS-2019_BBB

Dunn KJ, Bergman DJ, Latorraca GA (2002) Nuclear magnetic resonance: petrophysical and logging applications. Handbook of geophysical exploration. Pergamon, New York, pp 1–176

Gao FM, Xiao L, Zhang W, Cui WP, Zhang ZQ, Yang EH (2023) Low permeability gas-bearing sandstone reservoirs characterization from geophysical well logging data: a case study of Pinghu formation in KQT region, East China. Sea Process 11(4):1030. https://doi.org/10.3390/pr11041030

Green DP, Gardner J, Balcom BJ, McAloon MJ, Cano-Barrita PFJ (2008) Comparison study of capillary pressure curves obtained using traditional centrifuge and magnetic resonance imaging techniques. In: SPE Symposium on Improved Oil Recovery. https://doi.org/10.2118/110518-MS

Gui JY, Yin XY, Gao JH, Li SJ, Liu BY (2022) Petrophysical properties prediction of deep dolomite reservoir considering pore structure. Acta Geophys 70:1507–1518. https://doi.org/10.1007/s11600-022-00757-z

Hu ML (2021) Research on logging evaluation of effectiveness of sandstone conglomerate reservoir: taking Permian Jiamuhe Formation in Shawan Sag of Junggar Basin as an example. A Dissertation Submitted to China University of Geosciences for Master of Professional Degree, pp 1–68

Hucka V, Das B (1974) Brittleness determination of rocks by different methods. Int J Rock Mech Min Sci Geomech Abstr 11:389–392. https://doi.org/10.1016/0148-9062(74)91109-7

Jarvie DM, Hill RJ, Ruble TE, Pollastro RM (2007) Unconventional shale-gas systems: the mississippian barnett shale of north-central Texas as one model for thermogenic shale-gas assessment. AAPG Bull 91:475–499. https://doi.org/10.1306/12190606068

Jiang ZH, Mao ZQ, Shi YJ, Wang DX (2018) Multifractal characteristics and classification of tight sandstone reservoirs: a case study from the Triassic Yanchang formation, Ordos Basin, China. Energies 11(9):2242. https://doi.org/10.3390/en11092242

Jiang ZH, Li GR, Zhang LL, Mao ZQ, Liu ZD, Hao XL, Xia P (2022a) An empirical method for predicting waterflooding performance in low-permeability porous reservoirs combining static and dynamic data: a case study in Chang 6 formation, Jingan Oilfield, Ordos Basin, China. Acta Geophys. https://doi.org/10.1007/s11600-022-00990-6

Jiang ZH, Liu ZD, Zhao PQ, Chen Z, Mao ZQ (2022) Evaluation of tight waterflooding reservoirs with complex wettability by NMR data: a case study from Chang 6 and 8 members, Ordos Basin, NW China. J Pet Sci Eng 213:110436. https://doi.org/10.1016/j.petrol.2022.110436

Jin Y, Chen M, Zhang XD (2001) Determination of fracture toughness for deep well rock with geophysical logging data. Chin J Rock Mech Eng 20:454–456

Jin Y, Chen M, Wang HY, Yuan Y (2008) Study on prediction method of fracture toughness of rock model II by logging data. Chin J Rock Mech Eng 27:3630–3635

Jin XC, Shah SN, Roegiers JC, Zhang B (2015) An integrated petrophysics and geomechanics approach for fracability evaluation in shale reservoirs. SPE J 20:518–526. https://doi.org/10.2118/168589-PA

Kim SM, Mustafa MA, Reza GB (2019) A review of brittleness index correlations for unconventional tight and ultra-tight reservoirs. Geosciences 9:1–21. https://doi.org/10.3390/geosciences9070319

Kuang LC, Mao ZQ, Sun ZC, Xiao L, Luo XP (2010) A method of consecutively quantitatively evaluate reservoir pore structure by using NMR log data. China National Invention Patent

Li HT, Deng SG, Xu F, Niu YF, Hu XF (2021) Multi-parameter logging evaluation of tight sandstone reservoir based on petrophysical experiment. Acta Geophys 69:429–440. https://doi.org/10.1007/s11600-021-00542-4

Liang ZL, Cheng ZG, Dong XM, Hu TT, Pan T, Jia CM, Guan J (2021) A method to predict heterogeneous glutenite reservoir permeability from nuclear magnetic resonance (NMR) logging. Arab J Geosci 14:453. https://doi.org/10.1007/s12517-021-06840-x

Looyestijn WJ (2001) Distinguishing fluid properties and producibility from NMR logs. In: Proceeding of the 6th Nordic Symposium on Petrophysics, pp 1–9

Mao ZQ, Kuang LC, Sun ZC, Luo XP, Xiao L (2007) Effects of hydrocarbon on deriving pore structure information from NMR T_2 data. In: SPWLA 47th Annual Logging Symposium

Olubunmi A, Chike N (2011) Capillary pressure curves from nuclear magnetic resonance log data in a deep water Turbidite Nigeria Field - a comparison to saturation models from SCAL drainage capillary pressure curves. In: Proceeding of Nigeria Annual International Conference and Exhibition. https://doi.org/10.2118/150749-MS

Razaz M, Di ID, Wang BB, Asl SD, Thurnherr AM (2020) Variability of a natural hydrocarbon seep and its connection to the ocean surface. Sci Rep 10:12654. https://doi.org/10.1038/s41598-020-68807-4

Rickman R, Mullen M, Petre E, Grieser B, Kundert D (2008) A practical use of shale petrophysics for stimulation design optimization: all shale plays are not clones of the barnett Shale. In: Proceeding of SPE Annual Technical Conference and Exhibition. https://doi.org/10.1306/12190606068

Shao W, Ding Y, Liu Y, Liu S, Li Y, Zhao J (2009) The application of NMR log data in evaluation of reservoir pore structure. Well Logging Technol 33:52–56

Volokitin Y, Looyestijn WJ (2001) A practical approach to obtain primary drainage capillary pressure curves from NMR core and log data. Petrophysics 42:334–343

Wood DA (2022) Predicting brittleness indices of prospective shale formations from sparse well-log suites assisted by derivative and volatility attributes. Adv Geo-Energy Res 6:334–346. https://doi.org/10.46690/ager.2022.04.08

Xiao LZ, Li K (2011) Characteristics of the nuclear magnetic resonance logging response in fracture oil and gas reservoirs. New J Phys 13:045003. https://doi.org/10.1088/1367-2630/13/4/045003

Xiao L, Mao ZQ, Zou CC, Jin Y, Zhu JC (2016) A new methodology of constructing pseudo capillary pressure (*P*c) curves from nuclear magnetic resonance (NMR) logs. J Pet Sci Eng 147:154–167. https://doi.org/10.1016/j.petrol.2016.05.015

Xiao L, Mao ZQ, Li JR, Yu HY (2018) Effect of hydrocarbon on evaluating formation pore structure using nuclear magnetic resonance (NMR) logging. Fuel 216:199–207. https://doi.org/10.1016/j.fuel.2017.12.020

Xiao L, Li JR, Mao ZQ, Yu HY (2020) A method to evaluate pore structures of fractured tight sandstone reservoirs using borehole electrical image logging. AAPG Bull 104:205–226. https://doi.org/10.1306/04301917390

Ye YP, Tang SH, Xi ZD, Jiang DX, Duan Y (2022) A new method to predict brittleness index for shale gas reservoirs: Insights from well logging data. J Pet Sci Eng 208:109431. https://doi.org/10.1016/j.petrol.2021.109431

Yuan JL, Zhou JL, Liu SJ, Feng YC, Deng JG, Xie QM, Lu ZH (2017) An improved fracability evaluation method for shale reservoirs based on new fracture toughness prediction models. SPE J 22:1704–1713. https://doi.org/10.2118/185963-PA

Springer Nature or its licensor (e.g. a society or other partner) holds exclusive rights to this article under a publishing agreement with the author(s) or other rightsholder(s); author self-archiving of the accepted manuscript version of this article is solely governed by the terms of such publishing agreement and applicable law.